AD-A134 463 COMPARISON OF MEASURED AND COMPUTED BOUNDARY LAYERS AT 1/1
THE TAIL-END OF AN..(U) ADMIRALTY MARINE TECHNOLOGY
ESTABLISHMENT TEDDINGTON (ENGLAND.. G J COOPER JAN 83
UNCLASSIFIED AMTE(N)TM83053 DRIC-BR-89415 F/G 20/4 NL

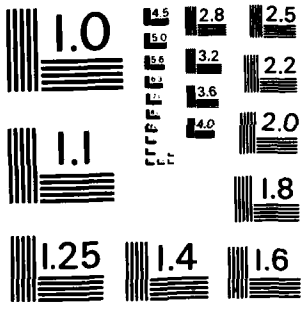

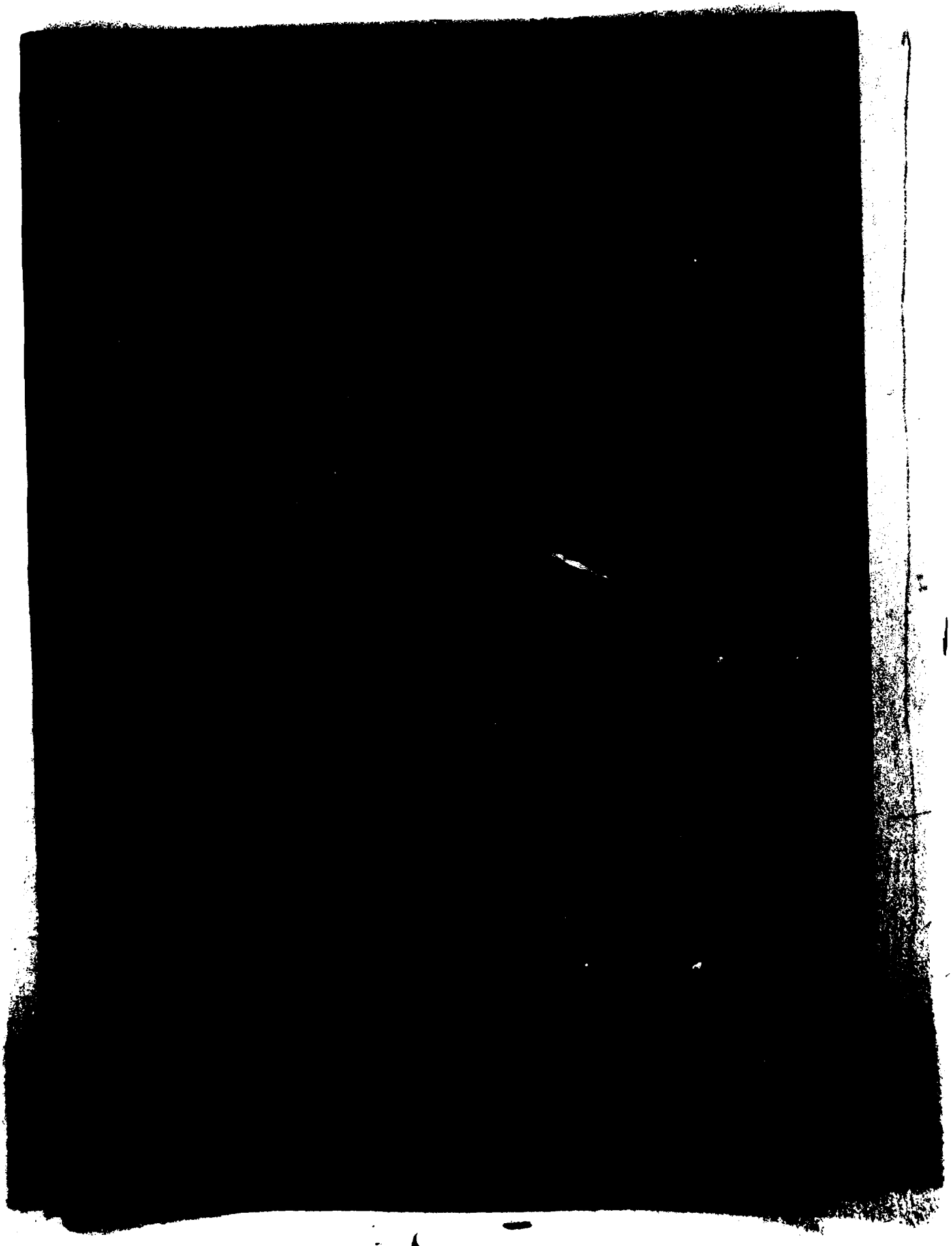

AMTE(N)TM83053

COMPARISON OF MEASURED AND COMPUTED BOUNDARY LAYERS AT THE TAIL-END OF AN AXISYMMETRIC BODY IN AN AIR JET

BY

G J COOPER

Summary

The limited range of Reynolds numbers achievable in low speed wind tunnels frequently prevents direct simulation of full scale flow fields. This problem is accentuated if it is required to model the flow over an underwater vehicle because of the widely differing kinematic viscosities of air and water. A tool is therefore required to predict the characteristics of air flows over models so that similarity with the full scale situation can be assessed.

The aim of this experimental study was to validate a theoretical model, developed earlier at AMTE Teddington, which predicts the potential flow and boundary layer development on an axisymmetric body placed in an open jet emerging from a nozzle.

The report describes the measurement of boundary layer velocity profiles at the tail-end of an axisymmetric body in an air jet, and compares the results with the predictions of the computer program. Results have been obtained for a variety of relative positions of the body and the jet exit, with the jet emerging from either a straight duct or a convergent nozzle. Good agreement is obtained in most cases, although for extreme positions of the body in the duct the calculated boundary layer thickness is smaller than the measured value by almost 15%.

The good agreement between measured and computed boundary layer parameters obtained in most cases gives confidence that the program can be used for determining future model test configurations for use in the Quiet Wind Tunnel, and for relating model data to full scale conditions. (U)

30 pages
12 Figures

AMTE (Teddington)
Queens Road
TEDDINGTON Middx TW11 OLN

January 1983

C O N T E N T S

LIST OF SYMBOLS

B	Constant in hot-wire response equation
C_p	Pressure coefficient
k	Hot-wire direction sensitivity coefficient
n	Constant in hot-wire response equation; index in boundary layer velocity profile law
r	Body radius
u, U	Flow velocity
U_o	Freestream flow velocity
u_1	Flow velocity at edge of boundary layer
U_{tan}	Flow velocity component tangential to body surface
V	Anemometer output voltage
V_o	Anemometer output voltage at zero flow
x	Axial distance from nose of body, +ve rearwards
y	Distance into boundary layer, normal to body surface
α	Angle of body surface to body axis
δ	Boundary layer thickness
δ^*	Boundary layer displacement thickness
Δ^*	Boundary layer displacement area
Δy	Small region in boundary layer (in equation 8)

INTRODUCTION

Wind tunnels are used for the testing of underwater bodies due to the cheapness of both the wind tunnel and the model compared to similar testing in water. However, the characteristics of air and water are such that the wind tunnel tests are often conducted at a Reynolds number which can be of the order of 100 times lower than the full scale situation it is intended to simulate. One way of overcoming this difficulty is to make the boundary layer profile and thickness (relative to some dimension such as hull radius) the same in the model test as in the full scale case. Geometrical changes can then be made and the effects on the flow assessed. This report describes some tests conducted with a small open jet wind tunnel to measure the effect of body position, in an air jet exhausting from a duct or nozzle, on the boundary layer at the tail-end of the body. Comparisons are then made between measured and computed results in order to demonstrate that a computer program developed at AMTE for calculating such flows can be reliably used to predict the flow field around models in the Quiet Wind Tunnel, a new facility at AMTE Teddington.

The computer program used was written in FORTRAN for an ICL 2970 computer. Input data to the program consists of nozzle and body coordinates, an initial estimate of the jet edge coordinates, the position of the boundary layer transition from laminar to turbulent flow and the Reynolds number. The output data gives potential flow profiles and boundary layer parameters at selected positions along the body.

2. APPARATUS

The wind tunnel is a straight-through type with an eight-bladed, axial flow fan. An aluminium alloy duct of 12 inches internal diameter was connected to the contraction outlet as illustrated in Figure 1. A nozzle 10 inches long could be attached to the duct outlet, reducing the outlet diameter to $10\frac{1}{2}$ inches. The axial and radial coordinates of the nozzle are given in Table 1. Flow velocity measurements could be made within the duct by passing hot-wire probes through a slot extending over most of the length of the duct and nozzle.

Two axisymmetric bodies were made from balsa wood with a cellulose lacquer (duraglaze) finish. Each model could be mounted by a tail sting on a support structure, illustrated in Figure 2, and its position relative to the duct or nozzle outlet adjusted longitudinally within limits set by the mounting support beam length and interference between the base block and the duct support. The body dimensions are given in Table 2, the smaller body having a maximum diameter of 6 inches and the larger body 8 inches. These dimensions have been used to distinguish between the models throughout this report.

The flow velocities were measured using two hot-wire anemometers, one of which was mounted on a traversing arrangment for measuring flow velocities around the body, the other being fixed at the upstream end of the duct for measuring the freestream velocity. Both hot-wire probes were X-probes for the measurement of velocity components in two orthogonal directions. The probes were connected to the inputs of a DISA 56C01/56C16 constant-temperature anemometer and the outputs from the anemometer were connected to a Hewlett-Packard Data Acquisition System controlled by a 9825B desktop computer. The measuring system is illustrated in Figure 3. Calibration of the hot-wire anemometer system is described in the Appendix.

The traversing arrangement consisted of a DISA 55E40 traversing mechanism driven by a 55B01 Sweep Drive Unit and a 55C01 External Stepping Motor giving a horizontal traverse perpendicular to the flow. This was mounted on a

carriage sliding along an optical bench standing on a rigid baseboard, allowing measurements parallel to the body axis.

3. TEST PROCEDURE

A particular model test configuration was selected and then set up. Measurements were made of the model's position within the duct and adjustments made until it was within 0.1 inch of that required. The traversing hot-wire probe was aligned with the model and set at a position which put the wires of the probe at the duct exit. This position was used as the datum for the measurement of the probe position along the model.

Both hot-wire probes were fitted into their probe bodies with their wire planes horizontal. The traversing probe body was positioned against the model's surface where the distance of the probe axis from the model axis could be accurately determined, and the traversing gear counter was set to the appropriate radial distance. The probe measuring freestream velocity was held by a retort stand and the probe inserted into the ducting upstream of the body until it was approximately one inch off the duct axis. The slot in the duct wall was taped over to prevent air escaping through it.

A velocity profile across half the duct is shown in Figure 4 for a flow velocity of 21ft/sec from which it can be seen that the probe measuring freestream velocity was well within the uniform flow region in the duct. It can also be seen that the peak velocity ratio shows a 6% difference in the velocities measured by the two hot wire probes. This is due to small differences in the calibration equations for the two probes. A factor was determined for each series of tests and the measured velocity ratios compensated for this discrepancy.

The flow speed was set to the required value 21ft/sec for the 6 inch body and 18ft/sec for the 8 inch body, giving a Reynolds number based on body length of 0.4×10^6 in both cases. These speeds were selected because some computed results were already available for this Reynolds number, and it was found that at higher speeds the velocity profile across the duct became very distorted. The data channels were scanned a specified number of times, typically ten, and the readings from each channel were arithmetically averaged. All subsequent calculations were performed upon these averaged values.

The output voltage from the DISA traversing gear was measured as a check on the probe position input manually to the program. The output voltages from the 55P63 probe measuring freestream velocity ahead of the model were converted to velocities using the calibration data stored in the program. The two velocities were arithmetically averaged to obtain the flow velocity in a longitudinal direction (relative to the probe axis) and the difference between them divided by two to obtain the flow velocity transverse to the probe axis.

The output voltages from each of the two wires of the 55P61 probe, measuring flow velocities around the body, were converted to effective cooling velocities using the stored calibration data. These two velocities and an initial estimate of the direction sensitivity coefficient k (discussed in the Appendix) were used to obtain a value of the resultant flow velocity. A more accurate value of k was then calculated and used with the measured voltages to obtain the final value of the resultant velocity. The direction of the flow was calculated relative to the probe axis, and hence the values of the axial and radial velocities, and the velocity tangential to the body surface, were calculated.

A value of pressure coefficient was calculated from the equation:

$$Cp = 1 - \left[\frac{U_{tan}}{U_o}\right]^2 \qquad (1)$$

where U_{tan} = velocity component tangential to the body surface

and U_o = freestream velocity.

The output data consisted of the traversing probe position, the velocity components described above, the angle of the resultant flow velocity to the body surface and the pressure coefficient. Additionally, the transverse component of the freestream velocity (the 55P63 probe being positioned to obtain a minimum reading) and each of the velocity components normalised by the longitudinal component of the freestream velocity were printed. After completion of measurements at each axial position all the measured probe voltages were listed for completeness. A typical output format is shown in Figure 5.

Measurements were made at intervals of 0.1 inch through the boundary layer at each axial station, and continued until either the velocity decayed, due to the probe reaching the mixing layer of the air jet, or a large region of constant velocity had been covered. The probe was then moved to another axial location for further measurements.

4. COMPUTER MODEL

The method used to calculate the potential flow field is based on the well-known surface singularity technique of Hess and Smith (1), and is described in full by Erith (2). The axisymmetric body is represented by an axial distribution of ring sources over its surface, and the nozzle and jet boundaries by distributions of ring vortices. The onset flow is assumed to be uniform at upstream infinity. The boundary conditions applied are those of zero normal velocity on the body surface and zero tangential velocity outside the nozzle and free jet boundaries. In addition the free jet boundary is a surface of constant pressure. The shape of this boundary is not known in advance, but must be determined as part of the solution. Hence an iterative procedure is necessary, in which an initial estimate is made of the jet boundary shape. The source and vortex strengths are then determined by applying the remaining boundary conditions, and the flow field is computed. If the assumed jet boundary shape does not coincide with a streamline of the flow then an adjustment must be made and the computation repeated. After convergence has been attained (generally in less than 20 iterations) the potential flow calculation is complete, and the program proceeds to the calculation of the boundary layer on the body surface.

The boundary layer computation is a first order one, ignoring any effect of the boundary layer on the potential flow. Furthermore, the boundary layer on the inner surface of the nozzle is neglected. The laminar portion of the boundary layer, from the front stagnation point to a prescribed transition station, is dealt with by the integral method of Pohlhausen (3). The turbulent boundary layer, which is of particular interest here, is calculated by the method of Myring (4). This uses a momentum integral equation and an equation involving the rate of entrainment of fluid into the boundary layer, both of which are

integrated along the body surface. Solution of this pair of simultaneous equations enables momentum area and a normalised shape parameter to be obtained for the boundary layer at positions along the body, and all other quantities of interest are obtained from these.

5. DATA ANALYSIS

5.1 Measured data

The measured boundary layer profiles were examined by plotting tangential velocity against distance from the body surface. An estimate of boundary layer thickness was then made by inspection of the profile and compared with the computed result.

In some cases a further comparison was made by calculating from the measured data a value for the displacement thickness, since this gave an indication of how well the measured and computed velocity profiles matched. The calculation of the displacement thickness from the measured data uses equations derived by Myring (4) in the form

$$\Delta^* = \delta^* \left(r + \frac{\delta^*}{2} \cos \right) \qquad (2)$$

and

$$\Delta^* = \int_0^{\delta} (y \cos \alpha + r) \left(1 - \frac{u}{u_1}\right) dy \qquad (3)$$

To calculate values from the measured data equation (3) was replaced by

$$\Delta^* = \sum_{i=1}^{i=j} (y_i \cos \alpha + r) \left(1 - \frac{u}{u_1}\right) \Delta y_i \qquad (4)$$

where Δy_i is the width of the ith element over which a measured velocity u_i is considered to act, and the summation is carried out over j elements in the boundary layer. With Δ^* found from equation (4) equation (2) was solved to obtain δ^*.

5.2 Computed data

For most of the experimental cases a computer simulation was performed using the program described in (2). In all the simulations a boundary layer transition station near the end of the hemispherical nose was used. This is considered to be reasonable since the flow from the wind tunnel is very turbulent and so ensures that the boundary layer becomes turbulent quickly.

The most immediately useful data were the potential flow profile and the boundary layer thickness since these could be compared with the flow measurement. The displacement thickness was compared with the value calculated from the measurements.

The computer output does not give explicitly any boundary layer velocity profile information and so it was necessary to calculate the profile from the data provided. It is assumed in the computation that the boundary layer profile is of the form

$$\frac{u}{u_1} = \left(\frac{y}{\delta}\right)^{1/n} \qquad (5)$$

where u is the flow velocity in the boundary layer at a distance y from the body surface,

δ is the boundary layer thickness, and

u_1 is the flow velocity at the edge of the boundary layer.

The index n of the power law must be evaluated for the profile to be defined.

For a flat plate the expression $n = \frac{\delta}{\delta^*} - 1$ is often used, but this is invalid for a rapidly tapering axisymmetric body where it is no longer possible to assume that the boundary layer thickness is small compared with the body radius. The following method was therefore used.

Equation (2), repeated below, shows that the displacement area Δ^* is defined by

$$\Delta^* = \delta^* \left(r + \frac{\delta^*}{2} \cos \right) \qquad (6)$$

where δ^* is the displacement thickness

r is the body radius, and

α is the angle of the body surface relative to its centreline.

If a power law velocity profile is assumed of the form of equation (5) then an alternative expression can be obtained:

$$\Delta^* = \frac{r\delta}{(1+n)} + \frac{\delta^2 \cos\alpha}{2(1+2n)} \qquad (7)$$

From the data given in the computer output and a knowledge of the body geometry it is possible to evaluate Δ^* from equation (6) and to use this in equation (7) to obtain a quadratic expression in n from which only one sensible solution can be obtained. Having evaluated n, a velocity profile in terms of u/u_1 is determined from equation (5) and this, with the computed ratio of the potential flow velocity to freestream velocity, is used to derive profiles of u/u_o for comparison with measurements.

6. RESULTS

Measured boundary layer profiles for the tests of the 6 inch diameter body are shown in Figures 6 and 7 for the convergent nozzle and straight duct configurations respectively. The three profiles in each figure were all measured at x = 32 inches, where the measurements are expected to be unaffected by the model's tail sting, but for different lengths of body inserted into the ducting, namely 10 inches, 18 inches and 26 inches. The boundary layer profile shapes appear to be typical of turbulent boundary layers, but it is evident that the boundary layer thickness cannot be accurately defined by simple inspection. Comparison of the boundary layer thickness derived from the measured data with that from the computations showed quite good agreement in most of the cases examined, of which only these six cases are shown. It should be noted that a variation of $\pm$ 0.1 inch in the measured boundary layer thickness is quite possible and represents a large variation as a percentage of the thickness even though only a small difference in magnitude.

The measured and calculated velocity profiles have some similarities in shape, the main difference is due to the measured velocity ratio outside the boundary layer being slightly greater than the calculated value for the convergent nozzle configuration. This is the result of the body boundary layer and the duct wall boundary layer forcing an increase in local velocity to achieve the necessary mass flow. This effect is not noticeable in the straight duct configuration. The difference in measured and computed velocity ratios outside the boundary layer were very small, the greatest being 4% of the measured value. The similarity between the measured and calculated velocity profiles is very good considering that methods for computing potential flows and integral properties of boundary layers have been used with an assumed power law for the boundary layer profile shape.

Figure 8 shows the variation of the measured and computed boundary layer thicknesses with axial body position. For the convergent nozzle configuration there appears to be a pronounced minimum in the variation of boundary layer thickness rather than the computed gradual decrease in thickness with the more rearward nozzle position, but the differences between measured and computed values are very small ($\pm$ 0.1 inch) and are probably due, in part, to measurement scatter. A similar situation is apparent with the straight duct configuration, for which two additional measurement points have been obtained to extend the curve. The measurements are consistent with the expectation that the boundary layer thickness at the tail of the body should reach a minimum for flow exit positions along the parallel portion of the body because of the increase in flow speed due to the blockage effect being a maximum. More data points would be required to demonstrate the existence of the minimum thickness by computation. The closest agreement between measured and computed boundary layer thicknesses occurs at flow exit positions situated away from the nose and tail of the body. The greatest differences occur at the most rearward flow exit positions and for the most rearward measurement position (x = 34 inches) where the difference approaches 15% of the measured value. As it is at the rear of the body that the first order boundary layer theory would break down, and there could also be sting effects in the measurements, the disagreement is not surprising.

The variations of measured and computed pressure coefficients along the 6 inch diameter body are shown in Figure 9 for both of the duct configurations. Pressure coefficient values are calculated using equation (1) where the value of tangential velocity is taken as the measured value near the boundary layer edge. The computed value is obtained using the potential flow velocity tangential to the body at the body surface and cannot be expected to give complete agreement with the measured values.

Examination of the major trends in the Figure shows reasonable agreement, particularly for the convergent nozzle case, although more extensive measurements are required around the beginning of the body taper (as for the 8 inch diameter model described later). The measured and computed velocities used in the pressure coefficient calculations (at the boundary layer edge and at the body surface respectively) differed by up to 10% of the measured values whereas the measured and computed velocities at identical positions outside the boundary layer differed by less than 4%.

The 8 inch diameter body was tested in the convergent nozzle and the variation of pressure coefficient along the body is shown in Figure 10. A corresponding velocity profile is shown in Figure 11. The pressure coefficient variation again shows good agreement in terms of the major features, including the peak at the

beginning of the body taper, except at the tail of the model. With this model the velocity profile, shown in Figure 11, illustrates that the boundary layer at the tail was incomplete due to merging with the jet mixing layer. This produced low velocities and hence less negative pressure coefficients relative to the computed flow field which did not account for this effect. It was evident that the 8 inch body was too big for use in the convergent nozzle and no further tests were made with this configuration.

After tests of the 6 inch body were completed a test of the 8 inch diameter model was made in the straight duct. A typical boundary layer is shown in Figure 12. It was concluded that the boundary layer could just achieve its full thickness before merging with the mixing layer. No further tests of the 8 inch diameter body were made.

7. CONCLUSIONS

This test program has indicated the range of boundary layer thicknesses which can be obtained by varying the position of a particular axisymmetric bo in a straight duct terminating with or without a convergent nozzle. It was found that the straight duct configuration produced thicker boundary layers than the convergent nozzle configuration due to the lower flow speed over the body. Measurements indicated that the boundary layer thickness at the tail of the body reached a minimum when the flow exit position was at some point along the parallel portion of the body, and this is as expected since the blockage effect of the body would be greatest. The measured trends are also present in the theoretical predictions, although the detailed variation of boundary layer thickness with flow exit position is not predicted precisely.

It has been shown that the computer program developed by Erith (2) can produce reasonably accurate values of the boundary layer thickness compared with the measured data, although there is difficulty in assessing the thickness from the measured velocity profiles. The difference between measured and computed boundary layer thickness is generally less than 10% of the measured value for most of the configurations studied. This error increases to around 15% very close to the tail of the body, but the higher error may be due to the breakdown of the first order boundary layer theory in this region and to sting interference.

Boundary layer velocity profiles have been derived from the computations and found to be very similar to the measured profiles. The measured and computed velocities at identical positions outside the boundary layer were found to be different by less than 4% of the measured value.

The variation of pressure coefficient along the body shows agreement in major trends between measurements and computations but gives different absolute values, reflecting differences in the velocities used in the calculations of up to 10%. However, complete agreement was not expected because of the two methods of calculating the pressure coefficient.

The results have shown that the program is a valuable aid in interpreting model test data, particularly in determining the similarity between model scale and full scale flows.

G J COOPER (HSO)

GJC/APG

APPENDIX

HOT-WIRE PROBE CALIBRATION

Two types of probe were used: a DISA Type x-probe for the measurement of the free stream velocity upstream of the model, and a DISA 55P61 x-probe for the measurement of the flow velocity around the model, the latter being a smaller probe on a longer stem making it more suitable for boundary layer measurements. Both types of probe were calibrated using the DISA 55D90 Calibration Unit, but the techniques used for each probe were different.

The calibration unit essentially consists of a nozzle to which a controllable supply of compressed air is connected. By varying the flow rate and nozzle area, ranges of flow velocity were covered to provide a relationship between the flow velocity and the probe output voltage. For the purposes of these tests a velocity range from 45m/s to 10m/s was covered with a $60mm^2$ nozzle and a range from 22.5m/s to 5m/s with a $120mm^2$ nozzle. The 55P63 probe was held by the calibration unit in its usual operating position relative to the flow direction and the output voltages from the two wires of the probe were noted for several flow velocities, from which a calibration equation was derived in the form

$$U = \frac{1}{B}\left(V^2 - V_o^2\right)^{1/n} \qquad (A1)$$

where U is the flow velocity from the nozzle,

V_o is the zero flow output voltage from the wire

V is the output voltage at velocity U m/s

and B and n are constants.

Correlation coefficients, indicating closeness of fit of the measured data to the mathematical expression, better than 0.999 were achieved.

The calibration of the 55P61 probe was done in a similar way except that voltage measurements were made at three orientations of the probe to the flow for each velocity setting. This enabled a more accurate determination of the flow direction to be determined when the probe was used to measure flow velocities at large angles to the model's axis. The first orientation of the probe was at a yaw angle of 45° to the flow, ie flow perpendicular to wire 1 and along wire 2; the second orientation was at a yaw angle of 0°, ie flow at 45° to both wires; the third orientation was at a yaw angle of -45°, ie flow along wire 1 and perpendicular to wire 2. After recording the measured output voltages in these three positions the probe was returned to the first position to check that the flow velocity had not fallen, due to lack of pressure in the supply, whilst measurements were being made.

A calibration equation was obtained for each wire using the output voltages measured when the flow was perpendicular to each wire. Again, correlation coefficients better than 0.999 were obtained. With the probe in this position the effective cooling velocity of the flow is the same as the actual flow velocity, but at other orientations a component of velocity along the wire exists which also has a cooling effect on the wire. This is usually ignored since it is a secondary effect if the yaw of the probe is small, as in the case of the 55P63 probe.

Having obtained a calibration of each wire's output voltage in terms of effective cooling velocity it was possible to evaluate a direction sensitivity coefficient k for each wire, hence relating the effective cooling velocity to the actual flow velocity by the use of an expression suggested by Hinze (5):

$$U_{eff}^2 = U_o^2 (\cos^2\alpha + k^2 \sin^2\alpha) \qquad (A2)$$

rather than the more usual cosine law which is

$$U_{eff} = U_o \cos\alpha \text{ (ie } k = 0) \qquad (A3)$$

where U_{eff} is the effective cooling velocity of the flow over the wire

U_o is the actual flow velocity

α is the inclination of the wire to the flow direction.

For the 55P61 probe the wires are set at $\pm 45^\circ$ to the probe axis so that a probe yaw angle of 45° puts one wire axis normal to the flow ($\alpha = 0^\circ$) and the other wire axis along the flow ($\alpha = 90^\circ$) as in the calibration procedure. The measured calibration results enable k to be evaluated since equation (A2) reduces to

$$U_{eff_o} = U_o \qquad \text{for } \alpha = 0^\circ$$

and

$$U_{eff_{90}} = k\, U_o \qquad \text{for } \alpha = 90^\circ$$

Hence

$$k = \frac{U_{eff_{90}}}{U_{eff_0}}$$

A value of the direction sensitivity coefficient was obtained at each flow velocity for each wire. From all these data a linear regression was carried out to obtain k as a function of velocity, a typical value of k being 0.25, decreasing slightly with increasing velocity. The correlation coefficient for the data for each wire was better than 0.9 in magnitude, but the data were combined resulting in a correlation coefficient of approximately 0.7. The use of a single relation between k and U_o for both wires of the probe was considered to be sufficiently accurate for the purposes of the present experiment. The final relationship for the direction sensitivity coefficient was put into the data logging program and used in the calculation of velocity.

REFERENCES

1. HESS, J.L. and SMITH, A.M.O. Calculation of Potential Flow about Arbitrary Bodies. Progress in Aeronautical Sciences 8, Pergamon Press 1966

2. ERITH, M.J. Axisymmetric Potential Flow past a Propelled Body in a Semi-infinite Duct. AMTE(N)R80103, October 1980

3. (ed) ROSENHEAD, L. Laminar Boundary Layers. O.U.P. 1963

4. MYRING, D.F. The Profile Drag of Bodies of Revolution in Subsonic Axisymmetric Flow. RAE TR72234, May 1973

5. HINZE, J.O. Turbulence. McGraw-Hill, 1959

Axial distance from exit plane (inches)	Radius (inches)
0.0	5.25
-0.5	5.35
-1.0	5.44
-1.5	5.52
-2.0	5.60
-2.5	5.67
-3.0	5.73
-3.5	5.79
-4.0	5.84
-4.5	5.88
-5.0	5.92
-5.5	5.95
-6.0	5.97
-6.5	5.99
-7.0	6.00
-7.5	6.00
-8.0	6.00
-8.5	6.00
-9.0	6.00
-9.5	6.00
-10.0	6.00

TABLE 1 INTERNAL SURFACE COORDINATES FOR CONVERGENT NOZZLE

6 INCH DIAMETER BODY

Axial distance from nose (inches)	Radius (inches)
0.0	0.0
0.0370	0.4689
0.1469	0.9272
0.3272	1.3618
0.5728	1.7630
0.8791	2.1209
1.2370	2.4272
1.6382	2.6728
2.0728	2.8531
2.5311	2.9630
3.00	3.00
26.00	3.00
26.25	2.9961
26.50	2.9819
26.75	2.9598
27.00	2.9291
27.50	2.8390
28.00	2.7142
29.00	2.4291
30.00	2.1429
32.00	1.5709
34.00	1.0000
34.50	0.8449
35.00	0.6551
35.25	0.5350
35.50	0.3780
35.65	0.2390
35.75	0.0

8 INCH DIAMETER BODY

Axial distance from nose (inches)	Radius (inches)
0.0	0.0
0.0488	0.6260
0.1961	1.2358
0.4358	1.8161
0.7642	2.3512
1.172	2.8280
1.6488	3.2358
2.1839	3.5642
2.7642	3.8039
3.3740	3.9512
4.00	4.00
29.00	4.00
29.25	3.9969
29.50	3.9870
29.75	3.9701
30.00	3.9461
30.50	3.8791
31.00	3.7858
31.50	3.6650
32.00	3.5240
34.00	2.9520
36.00	2.3811
38.00	1.8091
39.00	1.5240
40.00	1.2339
40.50	1.0689
41.00	0.8728
41.50	0.6169
41.90	0.2760
42.00	0.0

NB Both bodies were mounted on $1\frac{3}{4}$ inch diameter tail stings.

TABLE 2 SURFACE COORDINATES FOR AXISYMMETRIC BODIES

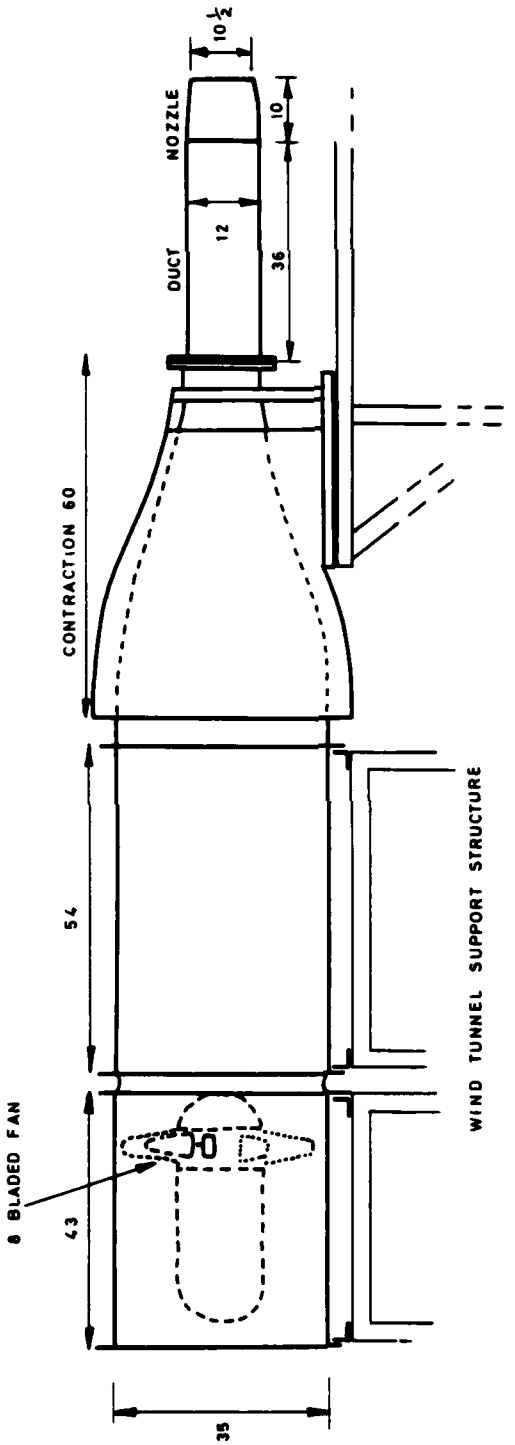

FIG. 1 GENERAL ARRANGEMENT DRAWING OF WIND TUNNEL
(Dimensions in inches)

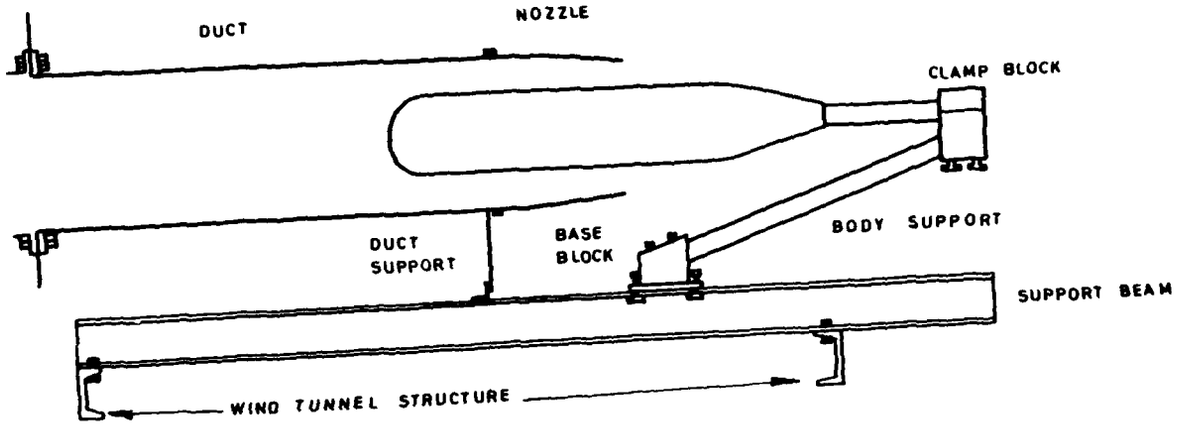

FIG. 2 BODY MOUNTING SYSTEM

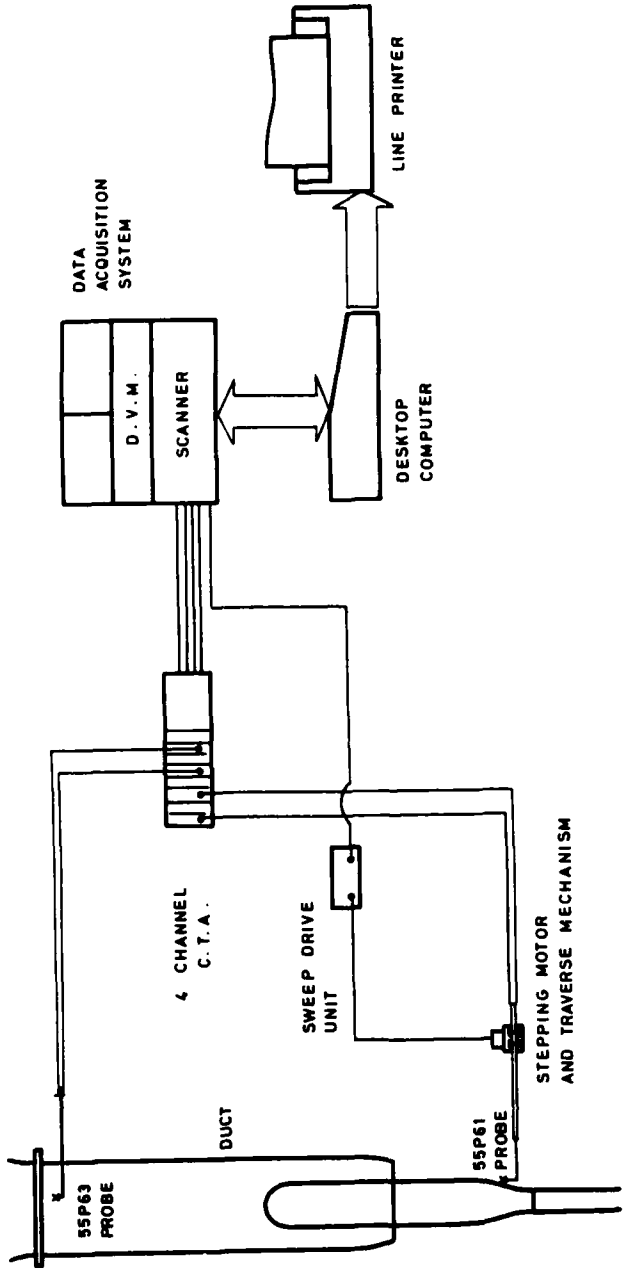

FIG. 3 MEASURING SYSTEM

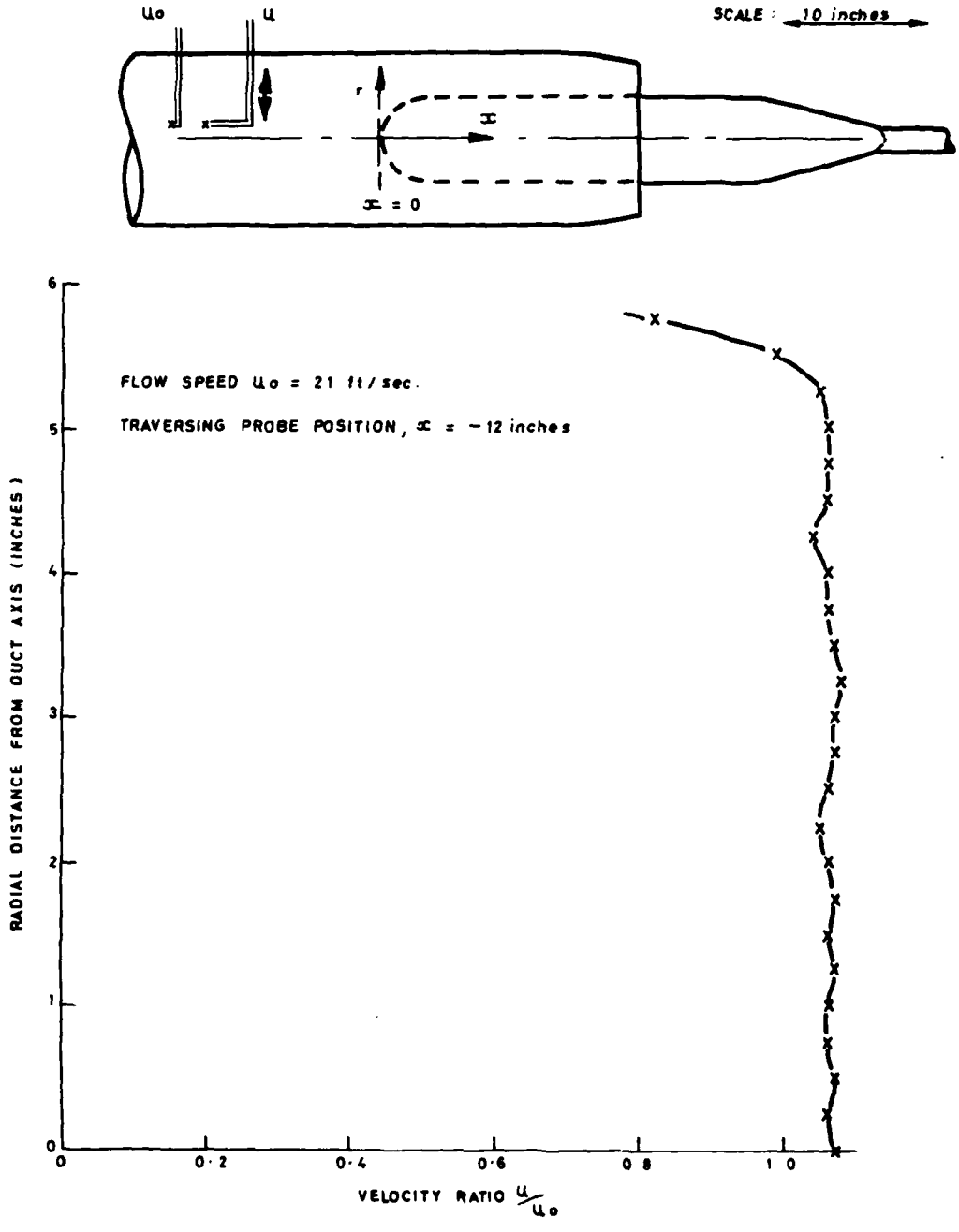

FIG. 4 VELOCITY PROFILE ACROSS DUCT

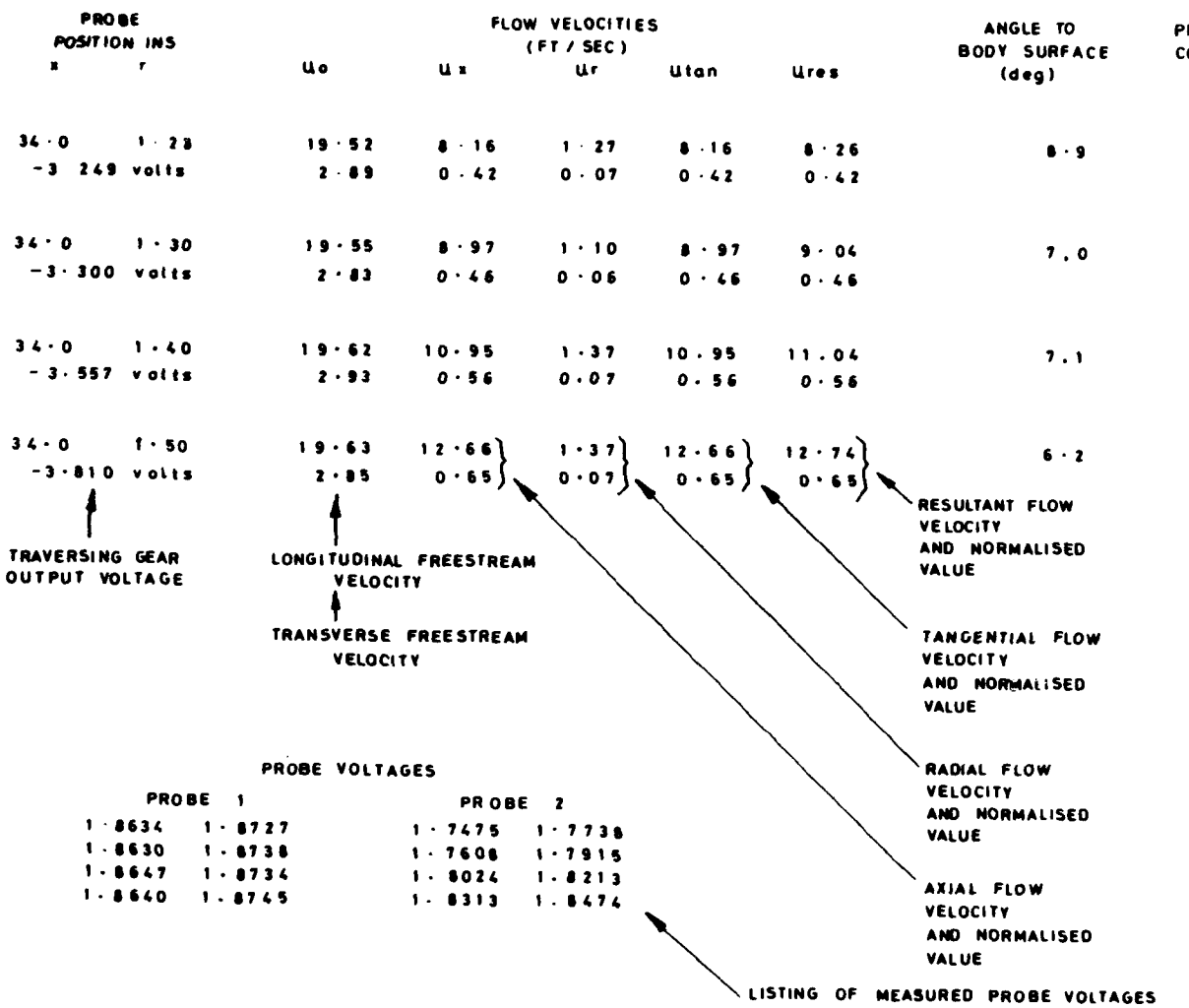

FIG. 5 SAMPLE OUTPUT

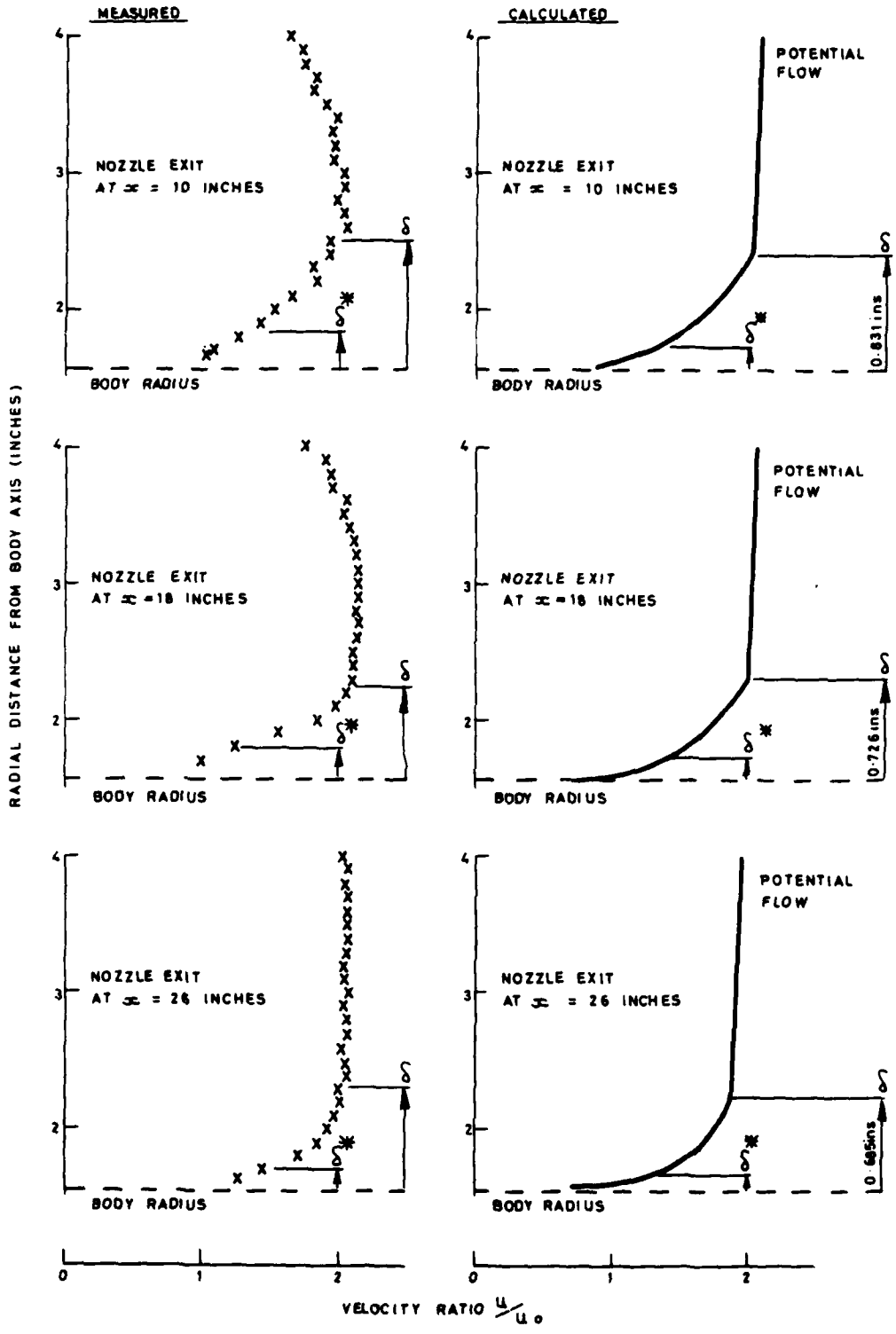

FIG. 6 6 INCH DIAMETER AXISYMMETRIC BODY AND CONVERGENT NOZZLE VELOCITY PROFILES AT x = 32 INCHES

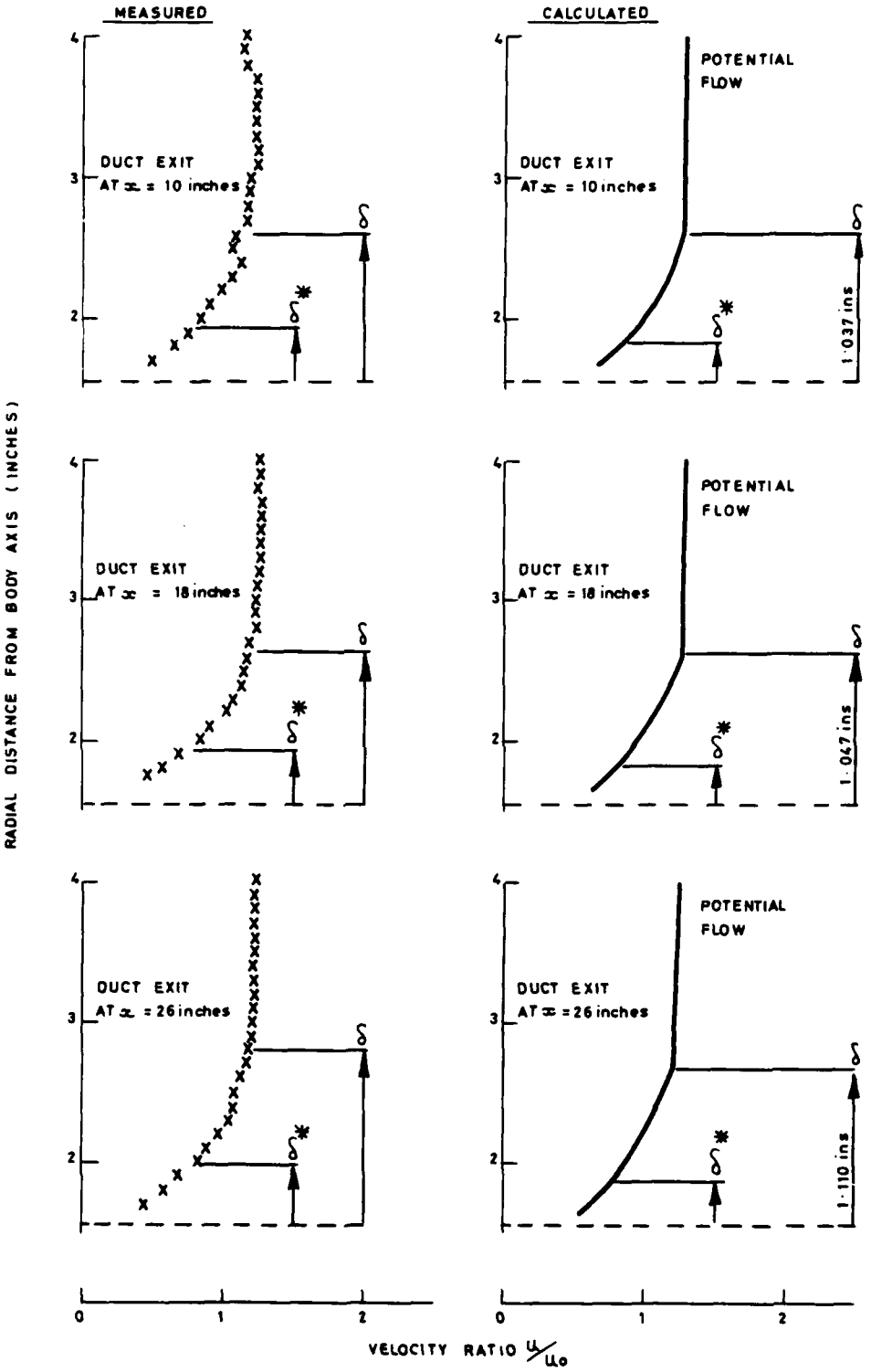

FIG. 7 6 INCH DIAMETER AXISYMMETRIC BODY AND STRAIGHT DUCT VELOCITY PROFILE AT x = 32 INCHES

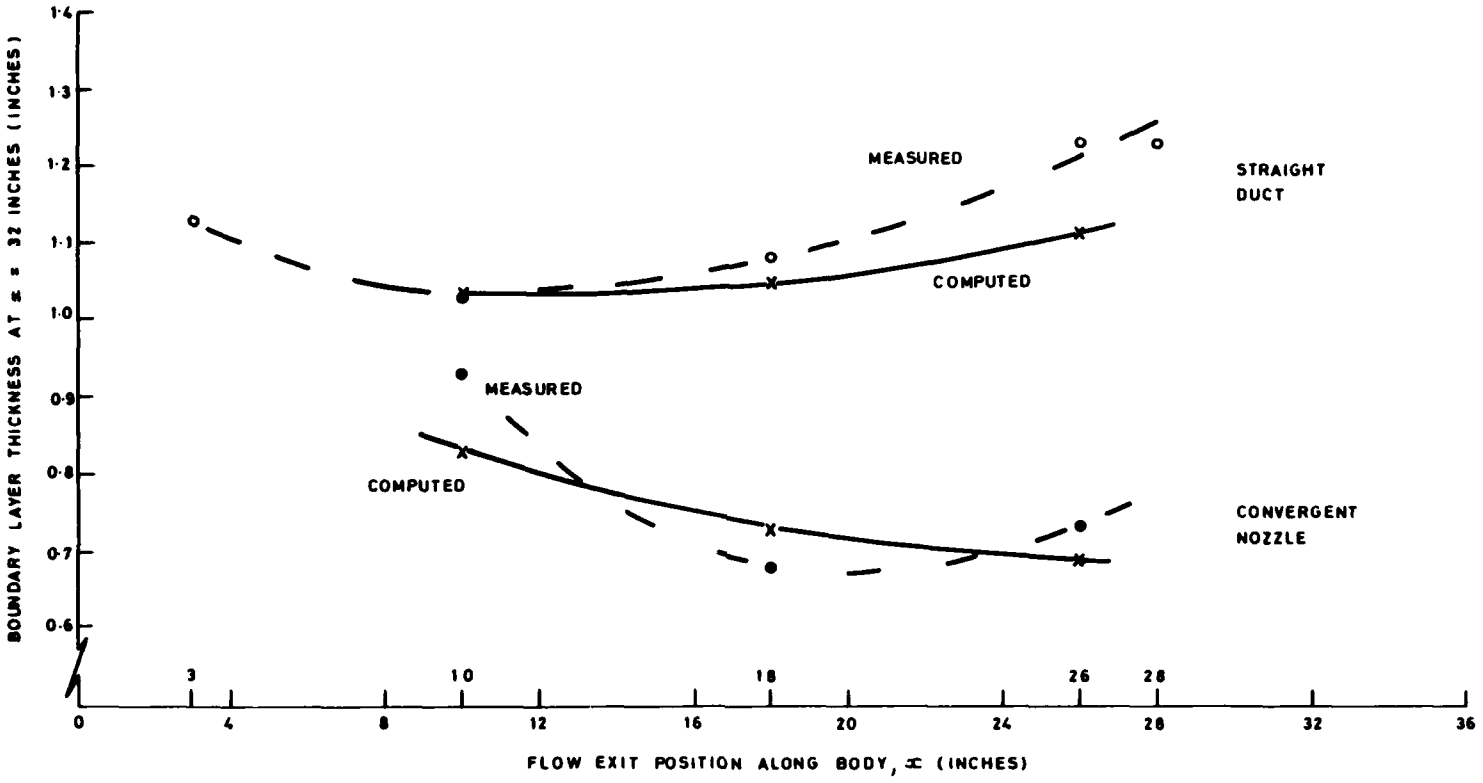

FIG. 8 VARIATION OF BOUNDARY LAYER THICKNESS WITH FLOW EXIT POSITION
6 INCH DIAMETER AXISYMMETRIC BODY

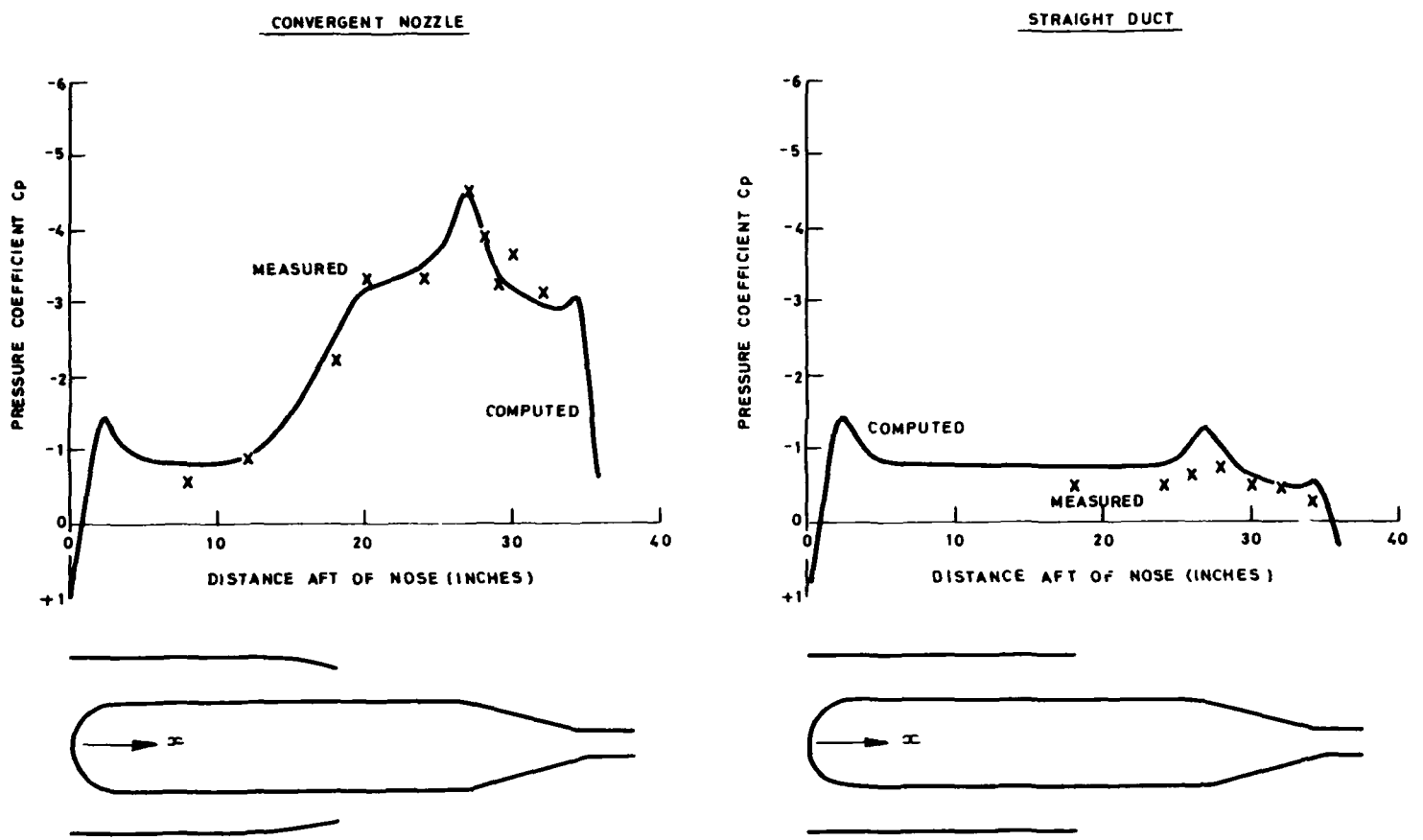

FIG. 9 VARIATION OF PRESSURE COEFFICIENT ALONG 6 INCH DIAMETER BODY

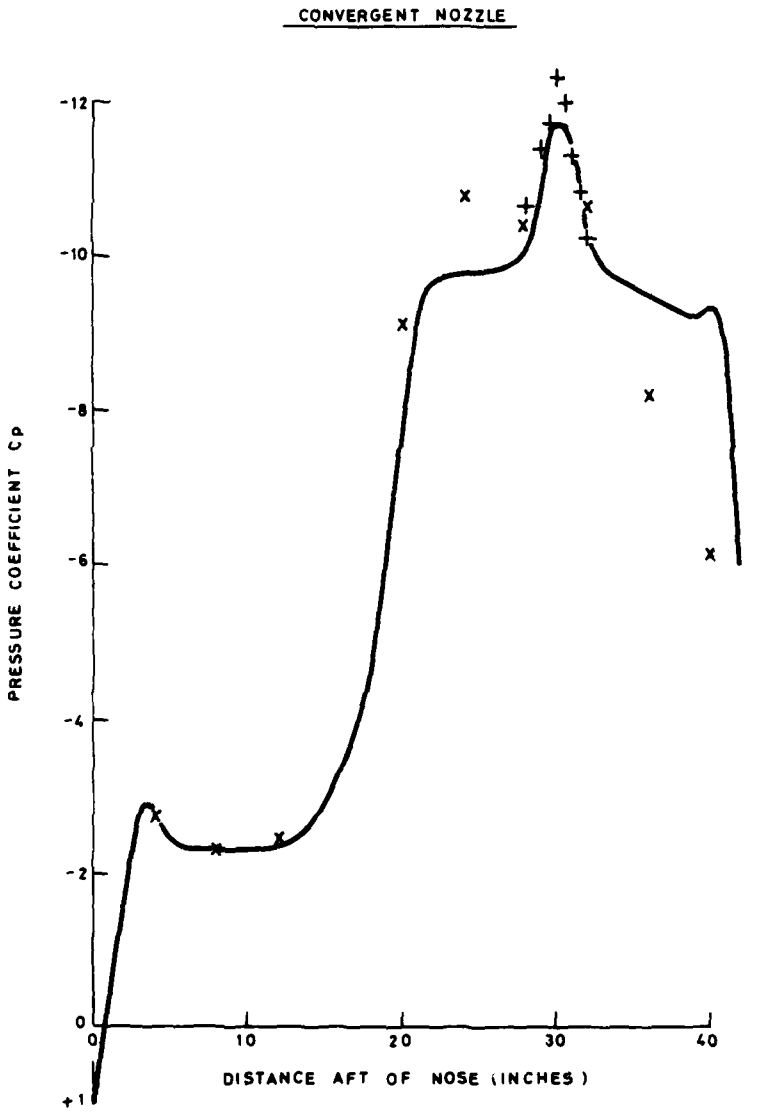

FIG 10 VARIATION OF PRESSURE COEFFICIENT ALONG 8 INCH DIAMETER BODY

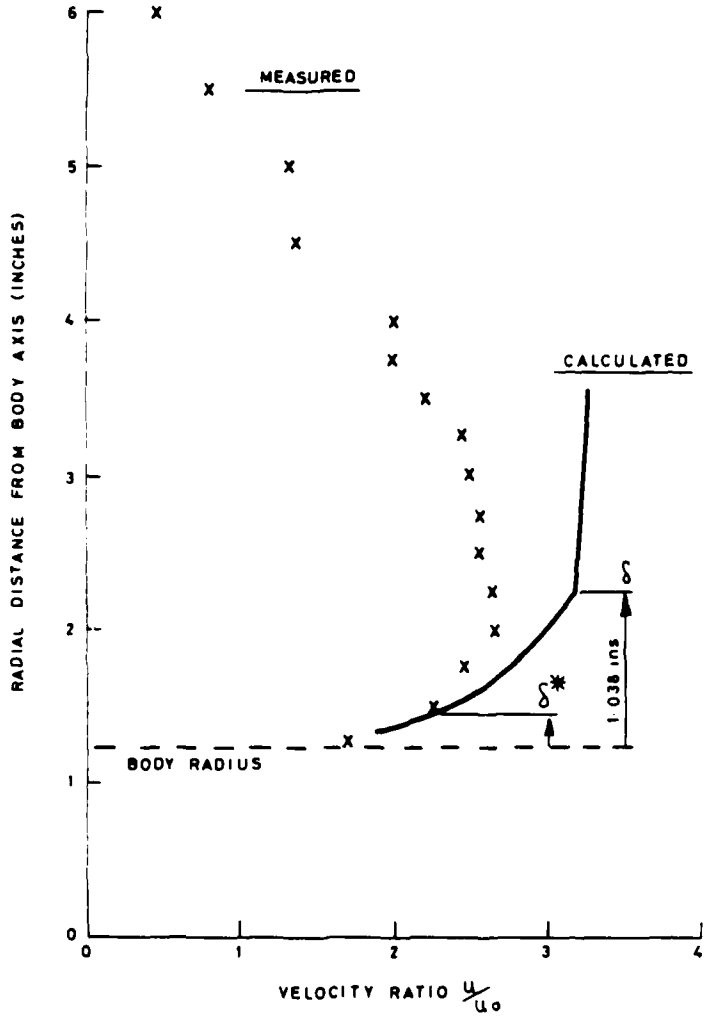

FIG. 11 8 INCH DIAMETER AXISYMMETRIC BODY AND CONVERGENT NOZZLE VELOCITY PROFILE AT x = 40 INCHES

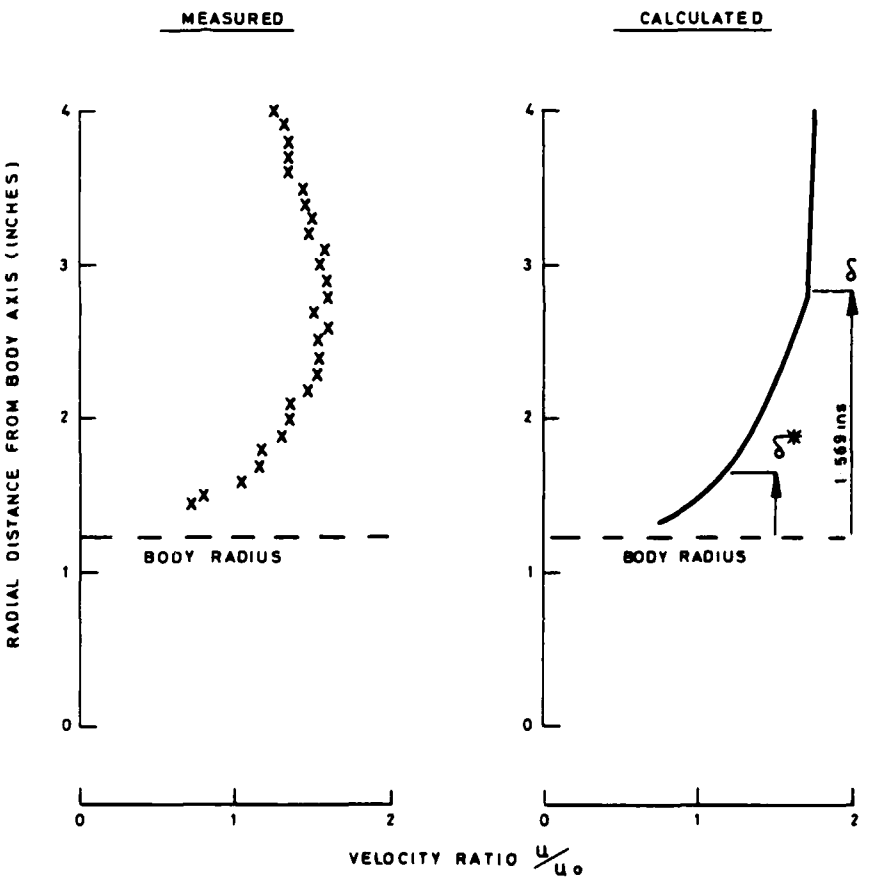

FIG. 12 8 INCH DIAMETER AXISYMMETRIC BODY AND STRAIGHT DUCT VELOCITY PROFILE AT x = 40 INCHES

END

DATE
FILMED

1283

DTIC